AMAE Int. J. on Production and Industrial Engineering, Vol. 4, No. 1, June 2013

Bifurcation Analysis of High-Speed Railway Vehicle in a Curve

M. Ranjbar[1], M. R. Ghazavi[2]
[1] Mechanical Engineering Department, School of Engineering, Tarbiat Modares University, Tehran, Iran
Email: ranjbar.mehdi88@gmail.com
[2] Mechanical Engineering Department, School of Engineering, Tarbiat Modares University, Tehran, Iran
Email: ghazavim@modares.ac.ir

***Abstract*— In order to prevent unpleasant incidents, preservation high-speed railway vehicle stability has vital importance. For this purpose, railway vehicle is modeled using a 38-DOF. This paper presents an investigation on limit cycle and bifurcation of high speed railway behavior. It is revealed that the critical hunting speed decreases by increasing the wheel conicity. Also the critical hunting speed and hunting frequency calculated via the linear elastic rail is higher than that derived using a nonlinear model.**

***Index Terms*— railway vehicle dynamics, heuristic nonlinear creep model, critical hunting speed, numerical simulation, bifurcation analysis.**

I. Introduction

The dynamic response of high-speed railway vehicles under rail loads is one of the fundamental problems to be solved in railway vehicles design and maintenance. With increasing speed, the lateral displacement of wheelset, can cause vibrations with large domain that called hunting (Fig. 1). Hunting is characterized by a limit cycle-type oscillation.

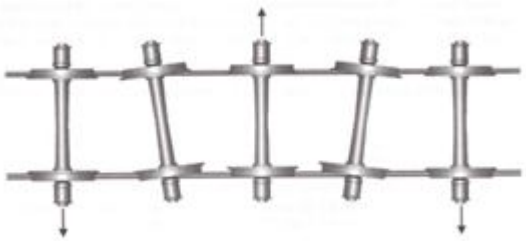

Figure 1. Hunting phenomena [1]

A lot of studies are performed on the stability and bifurcation analysis of railway vehicle. Based on the symbolic dynamic, Knudsen et al. [2, 3] performed bifurcation analysis in order to study the effects of the flange and suspension stiffness on the railway vehicle stability. Zeng and Wu [4] studied the effect of superelevation and curvature on the critical hunting speed with consideration 17-DOF and numerical methods. Zhai and Wang [5] presented a direct numerical method to determine the nonlinear hunting speed of railway vehicles. They investigated the difference between the rigid and elastic track model on the critical hunting speed. Based on a piecewise linear function and the Vermeulen-Johnson creep force laws, Gao et al. [6] determined the saddle node bifurcation point and the hopf bifurcation point for four-axle railway passenger car with consideration 17-DOF. Sedighi and Shirazi [7] investigated the influences of the system suspension nonlinearities and the wheel-rail interface nonlinearities on Hopf bifurcation.

In this paper, railway vehicle is modeled using a 38-DOF with consideration all possible motions (longitudinal, lateral, vertical, rolling, pitching and yawing). Investigation on limit cycle and bifurcation of high speed railway behavior is represented. Influence of wheel conicity and nonlinear elastic rail model on the bifurcation diagram is investigated. Finally, frequency power spectrum of the lateral displacement of the leading wheelset in the front bogie is represented.

II. Formulation Of Vehicle System

A. Railway vehicle model

In Fig. 2. schematic of vehicle system have been showed.

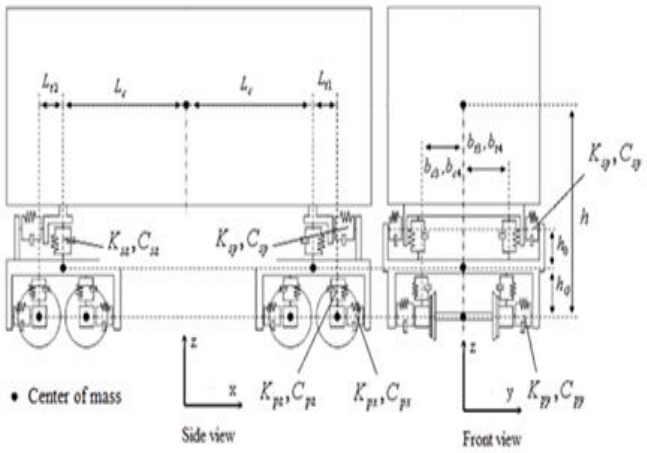

Figure 2. Schematic of vehicle system

In this Fig. the subscripts *p* and *s* indicate the primary and secondary suspension. The primary suspension connected the wheelsets and bogie frames and the secondary suspension connected the vehicle body and bogie frames. By considering all possible motions 6-DOF was defined for car body and 6-DOF was defined for each bogie frame. By considering constant rotation speed, one can neglect of the pitch motion of the wheelset around *y*-axis, so 5-DOF was defined for each wheelset (Fig. 3).

In this Fig. the subscripts *i* and *j* indicate the bogies location (*i*=1 for front bogie and *i*=2 for rear bogie) and the wheelsets location (*j*=1 for leading wheelset and *j*=2 for trailing wheelset). x, y, z, φ, γ and ψ are the longitudinal, lateral, vertical displacements, roll, pitch and yaw angles, respectively.

DOI: 01.IJPIE.4.1.1002

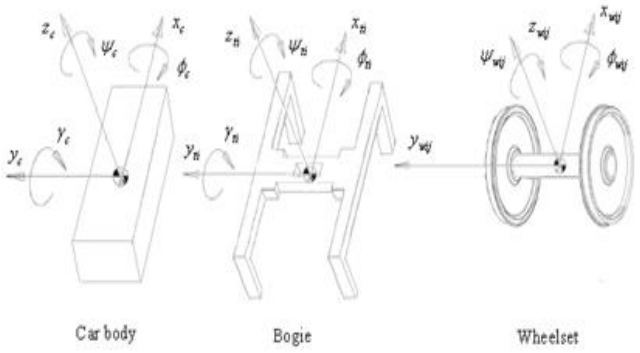

Figure 3. Degrees of freedom system

B. Wheel rail contact model

In this paper, two springs with high stiffness (K_{ry} for lateral stiffness and K_{rz} for vertical stiffness) are used to describe dynamic model for the rail.

The creep force and moment in the heuristic nonlinear creep model are represented as [8]

$$F^{n}_{pxij} = \alpha_{ij} F_{pxij}$$

$$F^{n}_{pyij} = \alpha_{ij} F_{pyij}$$

$$M^{n}_{pzij} = \alpha_{ij} M_{pzij}. \tag{1}$$

Where, the subscript P indicate the wheels location ($P = L$ for left wheel and $P = R$ for right wheel).

F_{Pxij}, F_{Pxij} and F_{Pzij} are the linear creep forces and moments, that define by transferring the Kalker's linear theory [9]. In the nonlinear creep formulation (1), the saturation constant α is represented in Ref. [10].

The normal forces are represented by

$$N_{Lzij} = -K_{rz}\left(z_{wij} - \lambda y_{wij} + a\varphi_{wij}\right)^{n}$$

$$N_{Rzij} = -K_{rz}\left(z_{wij} + \lambda y_{wij} - a\varphi_{wij}\right)^{n}$$

$$N_{Lyij} = -N_{Lzij}\tan\left(\delta_L + \varphi_{wij}\right)\cos\psi_{wij}$$

$$N_{Ryij} = N_{Rzij}\tan\left(\delta_R - \varphi_{wij}\right)\cos\psi_{wij}$$

$$N_{Lxij} = -N_{Lzij}\tan\left(\delta_L + \varphi_{wij}\right)\sin\psi_{wij}$$

$$N_{Rxij} = N_{Rzij}\tan\left(\delta_R - \varphi_{wij}\right)\sin\psi_{wij}. \tag{2}$$

Where, the constant n is the degrees of rail nonlinearity. The flange contact force can be represented by

$$F_{tij} = \frac{K_{ry}\left(y_{wij} - \delta\right)^{n}}{2}\left(\tanh\left(10^{4}\left(y_{wij} - \delta\right)\right) + 1\right) + \frac{K_{ry}\left(y_{wij} + \delta\right)^{n}}{2}\left(\tanh\left(10^{4}\left(-y_{wij} - \delta\right)\right) + 1\right). \tag{3}$$

III. Equations Of Motion

A. Car body and bogie frame

The equations of motion for the car body and bogie frame can be represented as follows

$$m_q \ddot{x}_q = F_{sxq}$$

$$m_q\left(\ddot{y}_q - \frac{V^2}{R_y}\right) = -m_q g\varphi_{se} + F_{syq}$$

$$m_q\left(\ddot{z}_q + \frac{V^2\varphi_{se}}{R_y}\right) = -m_q g + F_{szq}$$

$$I_{qx}\ddot{\varphi}_q = M_{sxq}$$
$$I_{qy}\ddot{\gamma}_q = M_{syq}$$

$$I_{qz}\ddot{\psi}_q = M_{szq}. \tag{4}$$

Where *c*, *t1*, and *t2* for the subscript *q* represent the vehicle body, the front bogie frame, and the rear bogie frame, respectively. The subscript s indicates the suspension force and moment that in order to short description, the detail of these suspension force and moment are not represented.

B. Wheelset

The equations of motion for the wheelset can be represented as follows

$$m_w \ddot{x}_{wij} = F^{n}_{Lxij} + F^{n}_{Rxij} + N_{Lxij} + N_{Rxij} + F_{sxwij}$$

$$m_w\left(\ddot{y}_{wij} - \frac{V^2}{R_y}\right) = -m_w g\varphi_{se} + F^{n}_{Lyij} + F^{n}_{Ryij} + N_{Lyij} + N_{Ryij} + F_{sywij} - F_{tij}$$

$$m_w\left(\ddot{z}_{wij} + \frac{V^2\varphi_{se}}{R_y}\right) = -m_w g + F_{Lzij} + F_{Rzij} + N_{Lzij} + N_{Rzij} + F_{szwij}$$

$$I_{wz}\ddot{\psi}_{wij} + \frac{I_{wy}V\dot{\varphi}_{wij}}{r_0} = R_{Rxij}F^{n}_{Ryij} - R_{Ryij}F^{n}_{Rxij} + R_{Lxij}F^{n}_{Lyij} - R_{Lyij}F^{n}_{Lxij} + R_{Rxij}N_{Ryij} + R_{Lxij}N_{Lyij} + M^{n}_{Lzij} + M^{n}_{Rzij} + M_{szwij}$$

DOI: 01.IJPIE.4.1.1002

$$I_{wx}\ddot{\varphi}_{wij} + \frac{I_{wy}V\left(\frac{V}{R_y} - \dot{\psi}_{wij}\right)}{r_0} = R_{Ryij}F_{Rzij} - R_{Rzij}F^{n}_{Ryij} + R_{Lyij}F_{Lzij} - R_{Lyij}F^{n}_{Lyij} + R_{Lyij}N_{Lzij} + R_{Ryij}N_{Rzij} - R_{Rzij}N_{Ryij} - R_{Lzij}N_{Lyij} + M_{Lxij} + M_{Rxij} + M_{sxwij}. \quad (5)$$

Where, the subscript w indicates the wheelset. R_{Pxij}, R_{Pyij} and R_{Pzij} are the components of the contact position vector on the wheels, that are represented in Ref. [9].

IV. Numerical Aspects

The equations (4) and (5) can be represented as

$$\dot{x}(t) = F\left(x(t)\right). \quad (6)$$

Where *x(t)* is a vector with 76-dimensional, and *F(x(t))* denote a nonlinear vector with 76-dimensional. In order to solve (6), zero initial condition, Runge-Kutta method of order four and the parameters values in Refs. [10-13] were used.

V. Result and discussion

A. Stable movement and corresponding limit cycle motion

Numerical simulations are performed with the linear elastic rail model (*n*=1). The lateral displacement phase portrait for the leading wheelset in the front bogie for velocities of motion equal 150(km/h) are represented in Fig. 4(a). One can conclude from this Fig. that the vibrations tend to the equilibrium point and stable motion reaches for freely long time behavior. By increasing velocity, the vibrations amplitude increase. For speeds less than the critical hunting speed, the vibrations go away after a long time. When velocities of motion reaches to 293(km/h), the system would not be stable. This speed is known as the critical hunting speed. For the critical hunting speed, results are shown in Fig. 4(b). In this Fig. the vibrations tend to the limit cycle for freely long time behavior. In fact, the limit cycle or hunting motion is occurred for first time. With velocities higher than the critical hunting speed, the limit cycle motion is preserved and the vibration amplitudes grow lightly for freely long time. For this purpose, results for velocities of motion equal 297(km/h) is illustrated in Fig. 4(c).

B. Bifurcation

In order to study motion at the freely long time, simulations were done for different velocities. For each velocity, lateral displacement of the leading wheelset drawn versus time. From this Fig. the value of maximum wheelst's lateral displacement read in the freely long time. Again, all these calculations are carried out for nonlinear elastic rail model (*n*=3). One can show these results in the bifurcation diagram (Fig. 5(a)). In this Fig. the dotted line, separate the stable movement from

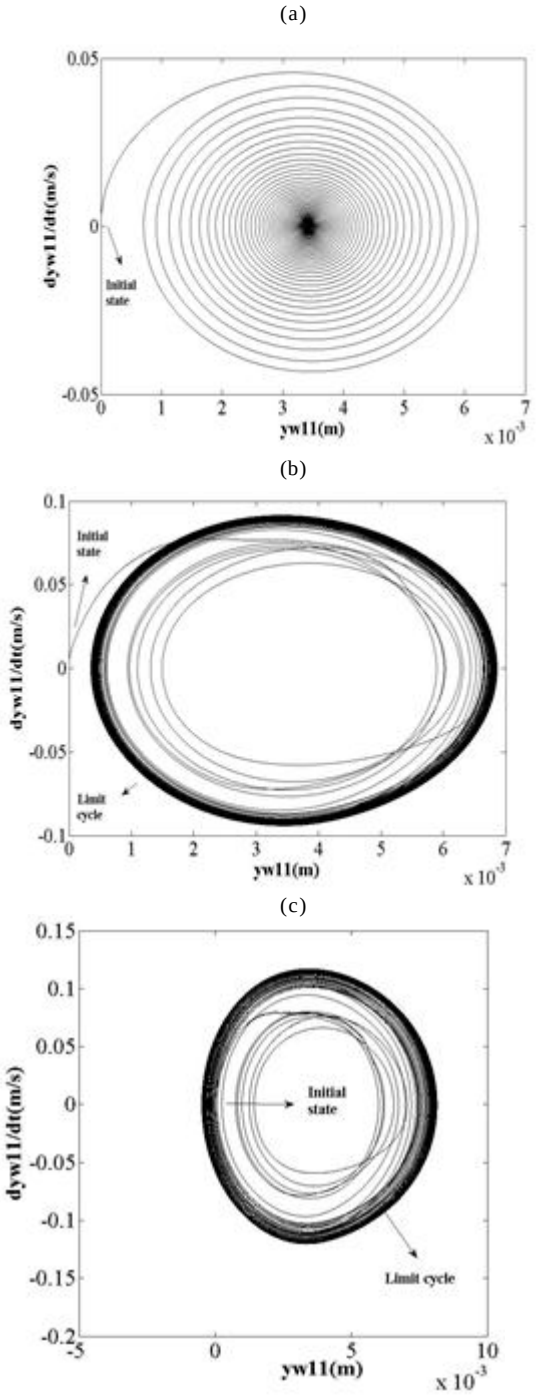

Figure 4. Phase portrait for velocities of motion equal (a) 150(km/h) (b) 293(km/h) (c) 297(km/h)

the limit cycle behavior. The speed correspond at the dotted line is the critical hunting speed. With study the bifurcation diagram, one can understand that critical hunting speed evaluated via the nonlinear elastic rail is lower than that derived using a linear model. This speed is 262(km/h) and 293(km/h) for the nonlinear and linear elastic rail model. In order to get higher critical speed, the linear elastic rail has advantage over nonlinear model.

Bifurcation diagram are drawn for linear elastic rail model and a range of wheel conicity (Fig. 5(b)). In this Fig. each monochromatic line Show bifurcation diagram for a particular

DOI: 01.IJPIE.4.1.1002

conicity. The critical hunting speed is 253(km/h), 280(km/h), 287(km/h) and 293(km/h) for wheel conicity 0.2, 0.1, 0.05 and 0.07, respectively.

Therefore the critical hunting speed decreases by increasing the wheel conicity. In curves, the outer rail will be a larger radius than the inner rail. This means that a cylindrical wheel has to travel further on the outer rail than on the inner rail. As the wheels moving on the inner and outer rail must have the same number of rotations per time unit such motion can not occur by pure rolling. To make the distances travelled by two wheels equal, both of them will therefore slip. The solution is to machine the rolling surface of wheels to a conical profile. By this reason, wheel conicity can not be zero. Therefore to get higher critical speed, the Small wheel conicity proposes.

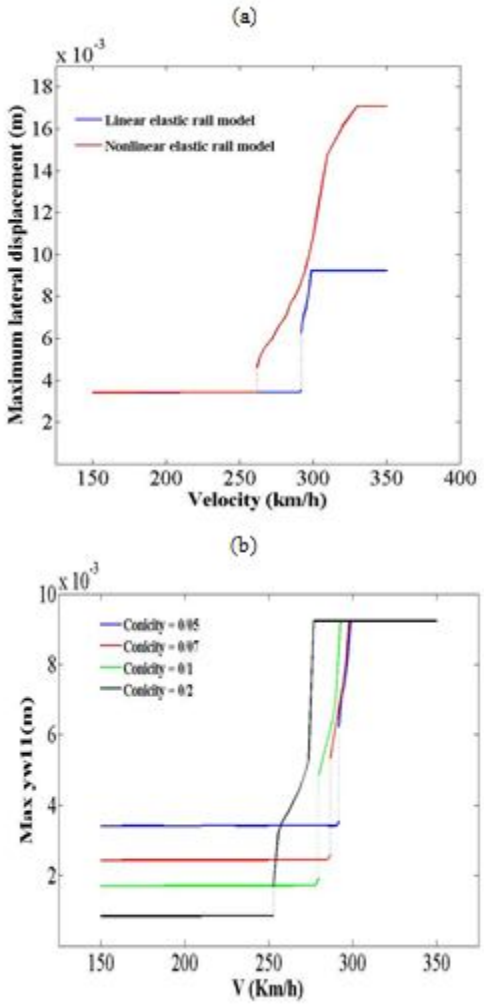

Figure 5. Bifurcation diagram for the lateral displacement of leading wheelset

C. *Frequency power spectrum*

In order to specify power spectrum of the lateral displacement of the leading wheelset in the front bogie, frequency analysis is carried out. The result is illustrated for the subcritical hunting speed (150(km/h)) in Fig. 6(a). As seen in this Fig. power spectrum increase with increasing frequency, until it reaches to the maximum value. Frequency in the maximum response is main frequency. In Fig. 6(a) main frequencies for the linear and nonlinear elastic rail model are 2.444 and 3 hertz, respectively. Result is illustrated for the critical hunting speed (Fig. 6(b)). Main frequencies for the linear and nonlinear elastic rail model are 4.778 and 4.333 hertz, respectively. This frequency is known as hunting frequency. These results reveal that the hunting frequency calculated via the linear elastic rail is greater than that derived using the nonlinear model. Frequency response for the supercritical hunting speed (297(km/h)) is illustrated in Fig. 6(c). In this Fig. main frequencies for the linear and nonlinear elastic rail model are 4.667 and 4.222 hertz, respectively.

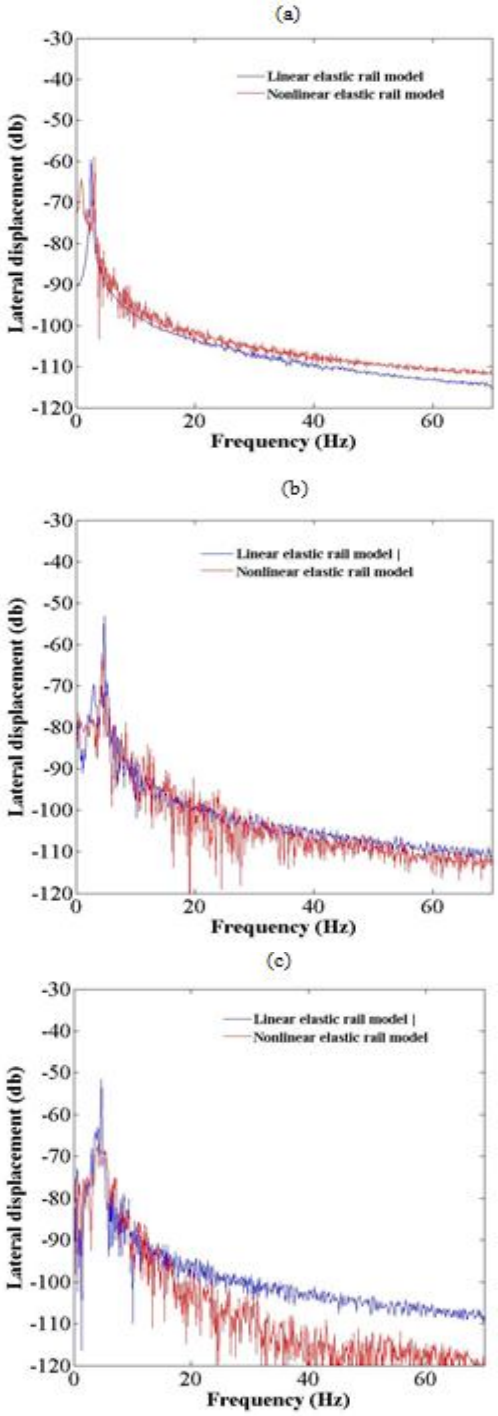

Figure. 6. Frequency power spectrum: (a) V= 150(km/h), (b) V= 293(km/h) and V=262(km/h) for the linear and nonlinear elastic rail model, respectively and (c) V=297(km/h).

DOI: 01.IJPIE.4.1.1002

Conclusions

In this research, a vehicle body, two bogie frames and two wheelsets for each bogie frame used to describe the railway vehicle model. The system dynamic modeled using a 38-DOF system including the longitudinal, lateral, vertical, roll, pitch and yaw displacements. Phase portraits are drawn to investigate stable movement and corresponding limit cycle motion. Runge-Kutta method used to solve dependent and nonlinear equations of motion. The long time behavior indicates that the vibrations tend to the equilibrium state for speeds lower than the critical hunting speed. Stable movement continues while speed is lower than critical hunting speed. When speed reaches to the critical hunting speed, limit cycle motion occur for first time. With velocities higher than the critical speed, the limit cycle motion is preserved and the vibrations amplitude grows lightly. In order to study stability, bifurcation analyses are performed. It is revealed that the critical hunting speed decreases by increasing the wheel conicity. Also the critical hunting speed and hunting frequency calculated via the linear elastic rail is higher than that derived using a nonlinear model. Therefore to get higher critical speed, the linear elastic rail model with small wheel conicity proposes.

References

[1] S. Iwnicki, *Handbook of railway vehicle dynamics.* CRC Press, 2006.

[2] C. Knudsen, R. Feldberg and H. True, "Bifurcations and chaos in a model of a rolling railway wheelset." *Philos. Trans. R. Soc. Lond. Ser. A*, vol. 338, pp. 1651. 455-469, 1992.

[3] C. Knudsen, E. Slivsgaard, M. Rose, H. True and R. Feldberg, "Dynamics of a model of a railway wheelset." *Nonlin. Dyn.*, vol. 6, pp. 2. 215-236, 1994.

[4] J. Zeng and P. Wu, "Stability analysis of high speed railway vehicles." *JSME Int J. Ser. C*, vol. 47, pp. 2. 464-470, 2004.

[5] W. Zhai and K. Wang, "Lateral Hunting Stability of Railway Vehicles Running on Elastic Track Structures." *J. Comput. Nonlin. Dyn.*, vol. 5, pp. 4. 2010.

[6] X. Gao, Y. Li and Q. Gao, "Lateral bifurcation behavior of a four-axle railway passenger car." *J. Appl. Mech.*, vol. 77, pp. 6. 2010.

[7] H. M. Sedighi and K. H. Shirazi, "Bifurcation analysis in hunting dynamical behavior in a railway bogie: Using novel exact equivalent functions for discontinuous nonlinearities." *Sci. Iran*, vol. 19, pp. 6. 1493-1501, 2012.

[8] D. Horak and D. Wormley, "Nonlinear stability and tracking of rail passenger trucks." *J. Dyn. Syst-T ASME*, vol. 104, pp. 256, 1982.

[9] R. Dukkipati, *Vehicle Dynamics.* CRC Press, 2000.

[10] P. Kim, J. Jung and J. Seok, "A parametric dynamic study on hunting stability of full dual-bogie railway vehicle." *Int. J. Prec. Eng. Manuf.*, vol. 12, pp. 3. 505-519, 2011.

[11] P. Kim and J. Seok, "Bifurcation analysis on the hunting behavior of a dual-bogie railway vehicle using the method of multiple scales." *J. Sound Vibrat.*, vol. 329, pp. 19. 4017-4039, 2010.

[12] S. Y. Lee and Y. C. Cheng, "Influences of the vertical and the roll motions of frames on the hunting stability of trucks moving on curved tracks." *J. Sound Vibrat.*, vol. 294, pp. 3. 441-453, 2006.

[13] S. Y. Lee and Y. C. Cheng, "A new dynamic model of high-speed railway vehicle moving on curved track." *J. Sound Vibrat.* , vol. 130, pp. 011009, 2008.

DOI: 01.IJPIE.4.1.1002